# Supplementary Information

# Nitrogen-Thermal Modification of the Bifunctional Interfaces of Transition Metal/Carbon Dyads for Reversible Hydrogenation and Dehydrogenation of Heteroarene

*Hui Su[a], Lu-Han Sun[a], Zhong-Hua Xue[a], Peng Gao[a], Shi-Nan Zhang[a], Guang-Yao Zhai[a], Yi-Ming Zhang[a], Yun-Xiao Lin[a], Xin-Hao Li*[a] and Jie-Sheng Chen[a]*

[a]School of Chemistry and Chemical Engineering, Shanghai Jiao Tong University, Shanghai 200240, P. R. China.

*Corresponding authors. E-mail address: xinhaoli@sjtu.edu.cn (X. H. Li).

# 1. Experimental section

## Materials

All chemicals were purchased from commercial sources without the further purification. Urea (Aladdin, 99%), cobalt (II) nitrate hexahydrate (Aladdin, 99.99 %), 1, 4-benzenedicarboxylic acid (Adams Reagent Co. Ltd, 99%), triethylene diamine (Aladdin, 98%), dimethylformamide (Aladdin, >99.9%), Cobalt oxide (Aladdin, 99%), quinoline (Aladdin, 99%), 1, 2, 3, 4-tetrahydroquinoline (Aladdin, 97 %), toluene (Acros, 99.85%, Extra Dry) was used a reaction solvent, $N_2$ gas (99.99%), $H_2$ gas (99.99%), Ar gas (99.99%).

## Method

The morphologies of Co/NC samples were examined by scanning electron microscopy (SEM) using a Nova NanoSEM 450 field emission scanning electron microscope (FEI, USA). The transmission electron microscopy (TEM) and high-resolution transmission electron microscopy (HRTEM) studies were performed on a JEM-2100F microscope operated at an acceleration voltage of 200 kV. Powder X-ray diffraction patterns (XRD) were collected on a Bruker D8 Advance X-ray diffractometer equipped with a Cu-Kα radiation source (λ = 1.5418 Å) and operated at a scan rate of 6° $min^{-1}$. The XPS measurements were conducted on a Thermo ESCALAB spectrometer using a monochromated Al Kα radiation (hv=1486.6 eV). The binding energy calibration of spectrometer was performed using C 1s peak at 284.8 eV. The UPS was recorded by at a Kratos Axis Ultra DLD spectrometer and ESCALAB 250 photoelectron spectrometer (Thermo Fisher Scientific). The metal elemental analysis was determined by inductively coupled plasma (ICP) measurements conducted on iCAP7600 spectrometer. The nitrogen adsorption/desorption test was performed at 77 K using Autosorb-iQA3200-4 sorption analyzer (Quantatech Co., USA) instrument. The specific surface area of sample was estimated by Brunauer-Emmett-Teller (BET) method. The desorption branch of isotherms was used to calculate pore size distribution by Barrett-Joyner-Halenda (BJH) method. $CO_2$-TPD analysis was carried out with AutoChem-Disvovery 2920 equipped with TCD signal. The sample (100 mg) was placed in a U-shaped quartz reactor and was pre-treated in He flow at 150 ℃ for 2h and cooled to room temperature. After being saturated with $CO_2$, the sample was purged with He for 2h at room temperature to sweep the physical molecule. Then sample was heated by 700 ℃ at the rate of 15 ℃/min. The signals were monitored by a thermal conductivity detector (TCD). 1, 2, 3, 4-tetrahydroquinoline gas TPD measurement was performed with AutoChem-Disvovery 2920 equipped

with TCD signal. The samples (100 mg) was treated in He flow at 250 ºC for 0.5 h and cooled to room temperature. Subsequently, sample was purged with He for 2h. The desorbed temperature was from 50 ºC to 250 ºC with a heat rate of 15 ºC/min. The desorbed products was determined by TCD. Gas chromatography (GC) analysis was conducted on SHIMADZU GC-2014C GC system (Japan) equipped with Rtx-5 column (30 m x 0.25 μm x 0.25 μm). Gas chromatography-mass spectrometry (GC-MS) analysis was carried out on SHIMADZU GCMS-QO2010 SE (Japan) equipped with Rtx-5 Sil MS column (30 m x 0.25 μm x 0.25 μm).

**XAFS measurements**

The X-ray absorption data at the Co K-edge of the samples were collected at beamline BL14W1 of the Shanghai Synchrotron Radiation Facility (SSRF). The station was operated with a Si (111) double crystal monochromator. The synchrotron was operated at 3.5 GeV and the current was between 150-210 mA. The data for each sample were recorded in transmission mode using ion chambers and calibrated with standard Co metal foil at ambient conditions. As-acquired data was processed via standard procedures using the program ATHENA. The curve fittings of extended X-ray absorption fine structure (EXAFS) spectra were conducted using the ARTEMIS module of IFEFFIT.

**Preparation of polymeric carbon nitride (PCN)**

According to our previous reports, [10c, 15a] urea was added into crucible and heated up to 550 °C with a heating rate of 2.3 °C/min for 4 h in air atmosphere.

**Preparation of $Co_x/N_yC$**

Cobalt (II) nitrate hexahydrate (0 g, 0.584 g, 1.168 g, 2.336 g or 3.504 g), 1,4-benzenedicarboxylic acid (2.72 g) and triethylene diamine (1.92 g) were mixed into N,N-dimethylformamide (150 ml) for the synthesis of $N_{0.17}C$, $Co_{0.08}/N_{0.14}C$, $Co_{0.14}/N_{0.11}C$, $Co_{0.23}/N_{0.10}C$ or $Co_{0.3}/N_{0.06}C$. Then, polymeric carbon nitride powder (18.56 g) was dispersed with the as-obtained cobalt-containing complex slurry. The mixture was stirred and dried at 120 °C. The as-prepared solid powder was heated up to 900 °C at a heating rate of 1.5 °C/min under $N_2$ gas flow. The temperature of the aforementioned nitrogen thermal reaction was maintained at 900 °C for 1 h.

**Preparation of $Co/NC-H^+$**

The nonoxidative acid-etching of $Co_{0.08}/N_{0.14}C$, $Co_{0.14}/N_{0.11}C$, $Co_{0.23}/N_{0.10}C$ or $Co_{0.3}/N_{0.06}C$ (60 mg) was carried out in a 10 M HCl solution at 90 °C for 24 h and repeated 3 times. The washing of the

resultant sample was conducted using deionized water, and the sample was finally dried at 60 °C for the following characterizations and catalytic reactions.

**Catalytic hydrogenation of quinoline under solvent-free conditions**

A mixture of $Co_x/N_yC$ catalysts (containing 0.16 mol % Co species; $Co_{0.08}/N_{0.14}C$, 52 mg; $Co_{0.14}/N_{0.11}C$, 30 mg; $Co_{0.23}/N_{0.10}C$, 18 mg; $Co_{0.3}/N_{0.06}C$, 14 mg) and quinoline (44 mmol) were added into a 100 mL stainless-steel autoclave (BERGHOF Products + Instruments GmbH, Germany) with a stir bar. The autoclave was washed with pure hydrogen gas 3 times, pressurized to 30 bar $H_2$ and placed into an aluminum block. The reaction vessels were preheated to 120 °C after 45 minutes and then stirred (1000 r.p.m) for 4 h, followed by cooling to room temperature. After the completion of the reaction, the collection of catalysts was performed by filtration and the crude liquid mixture was diluted with ethyl acetate, followed by GC-MS and GC analysis.

**Hydrogenation of quinoline under solvent conditions**

A mixture of $Co_{0.14}/N_{0.11}C$ catalysts (20 mg), toluene (4 mL) and quinoline (0.5 mmol) was added into a 100 mL stainless-steel autoclave. The autoclave was washed with pure hydrogen gas 3 times, pressurized to 5 bar $H_2$ and placed into aluminum block. The reactor was heated to 120 °C after 45 minutes and then stirred (1000 r.p.m) for 16 h, followed by cooling to room temperature. The product was analyzed by GC-MS and GC.

**Catalytic dehydrogenation of 1, 2, 3, 4-tetrahydroquinoline**

First, 100 mg of the catalysts ($N_{0.17}C$, $Co_{0.08}/N_{0.14}C$, $Co_{0.14}/N_{0.11}C$, $Co_{0.23}/N_{0.10}C$ or $Co_{0.3}/N_{0.06}C$), 1, 2, 3, 4-tetrahydroquinoline (0.5 mmol) and toluene (10 mL) were mixed in a 100 mL stainless-steel autoclave reactor (BERGHOF Products + Instruments GmbH, Germany). After purging by argon gas three times, the sealed autoclave was pressurized with argon gas (30 bar) and heated from room temperature to 160 °C over 45 minutes. The reaction vessel was vigorously stirred (1000 r.m.p) for 12 h or (4, 8, 12, 16, 24, 36, or 48 h). After completion of the reaction, the reactor was cooled to room temperature and the crude liquid-phase mixture was analyzed by GC-MS and GC.

**Reversible dehydrogenation-hydrogenation cycle testing**

Reversible dehydrogenation-hydrogenation cycle testing was conducted in a 100 mL autoclave sealed by pure argon or hydrogen gas. In the initial dehydrogenation reaction, $Co_{0.14}/N_{0.11}C$ catalysts (100 mg), toluene (10 mL) and 1, 2, 3, 4-tetrahydroquinoline (0.1 mmol) were added to the utoclave. After

purging for three times with argon gas, the autoclave was pressurized with argon gas (30 bar) and heated to 160 °C after 45 minutes. Then the reaction vessel was stirred (1000 r.m.p) at 160 °C for 8 h. In the hydrogenation reaction, 5 bar of $H_2$ was used to pressurize the autoclave, and the sample was heated to 120 °C over 45 minutes with stirring (1000 r.m.p). The reactor temperature was maintained for 4 h. Dehydrogenation reaction time was prolonged to 48 h in the 2nd $H_2$ release/storage cycle. After 2 cycles, the final catalyst was separated by centrifugation and washed with pure toluene for structural characterization.

**Density functional theory calculation details**

The first-principles density functional theory calculations were carried out using the Dmol3 module in Material Studio. The simulation of $Co_x/N_yC$ catalysts was optimized using a $Co_4$ cluster placed on a (6×6) graphene sheet (a=b=14.76 Å and $\gamma$=120˚) (Fig. S15). 15 Å vacuum space between sheets was applied to separate contiguous slabs. The concentration of N atoms and the ratio of pyrindic and graphitic nitrogen in the $Co_x/N_yC$ model was close to the variation tendency based on the XPS results (Table S1 and Fig. S10). The electronic exchange-correlation energy was described by the generalized-gradient approximation (GGA) with the Perdew-Burke-Ernzerhof (PBE) with TS dispersion correction[S1] to optimize the $Co_x/N_yC$ model. The double numerical plus polarization (DNP) was used as the basis set, and the DFT Semicore Pseudopots method was employed for core treatment.[S2-3] The k-point was specified 6×6×1 using the Monkhorst-Pack grid. The binding energy between the H -atom and Co/NC was defined as the following equation:

$$E_b = \frac{1}{2}E_{H2} + E_{Co/NC} - E_{H-Co/NC}$$

where $E_{H_2}$, $E_{Co/NC}$, and $E_{H-Co/NC}$ are the total energies of the $H_2$, Co/NC system, and H atom absorbed on Co/NC respectively.
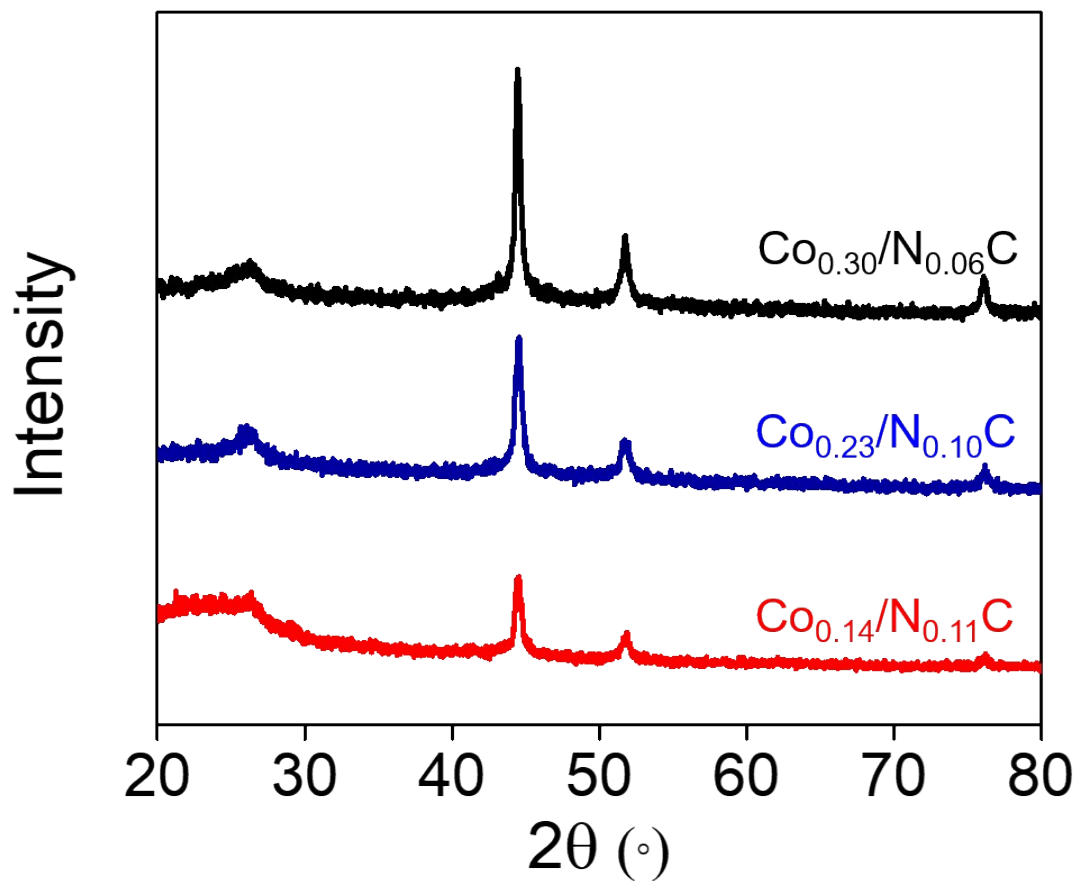
**Fig. S1**. Power XRD profiles of $Co_{0.14}/N_{0.11}C$ (red line), $Co_{0.23}/N_{0.10}C$ (blue line) or $Co_{0.3}/N_{0.06}C$ (black line). The typical peaks were assinged to cubic cobalt component.
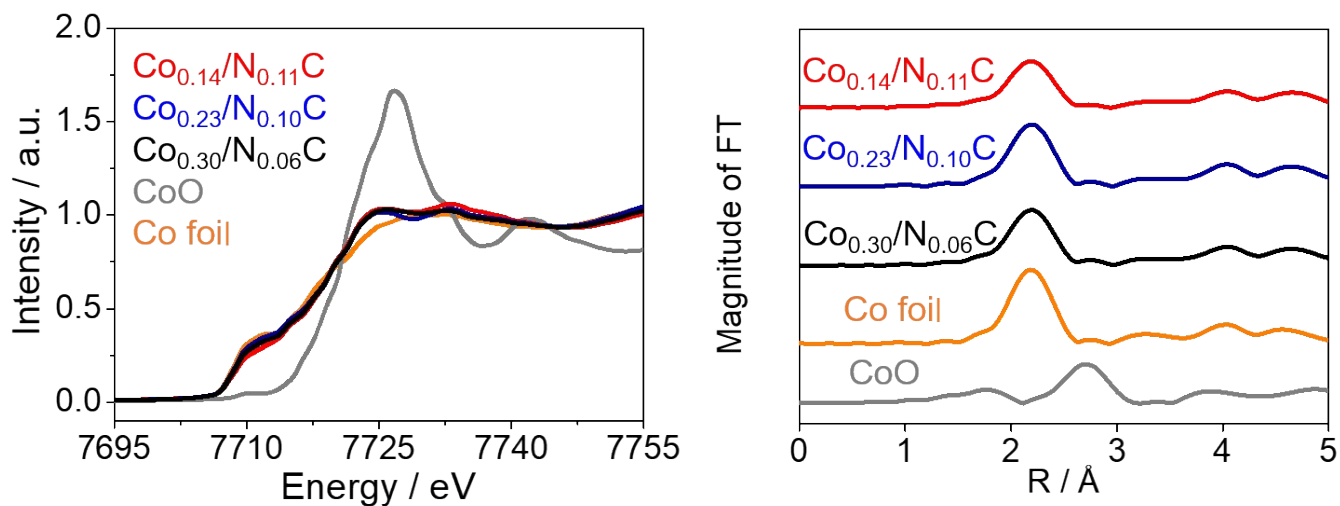
**Fig. S2**. Normalized XANES spectra and the corresponding Fourier-transformed EXAFS spectra of Co/NC samples Co foil and CoO at the Co K-edge. The peak at 2.2 Å in Fourier-transformed EXAFS spectra corresponds to the Co-Co coordination, demonstrating the metallic feature of cobalt component.
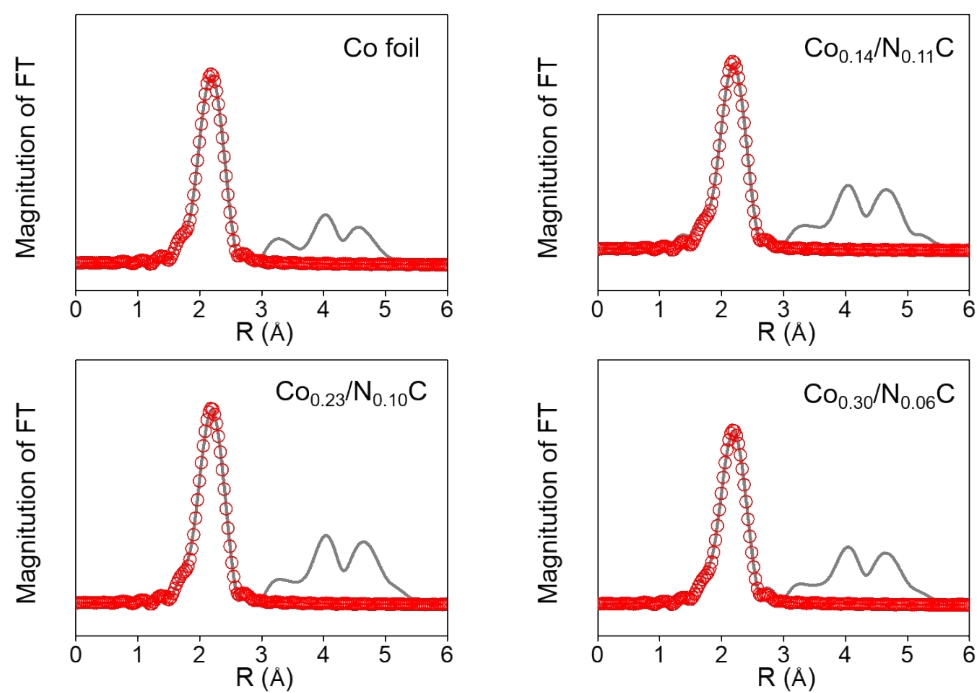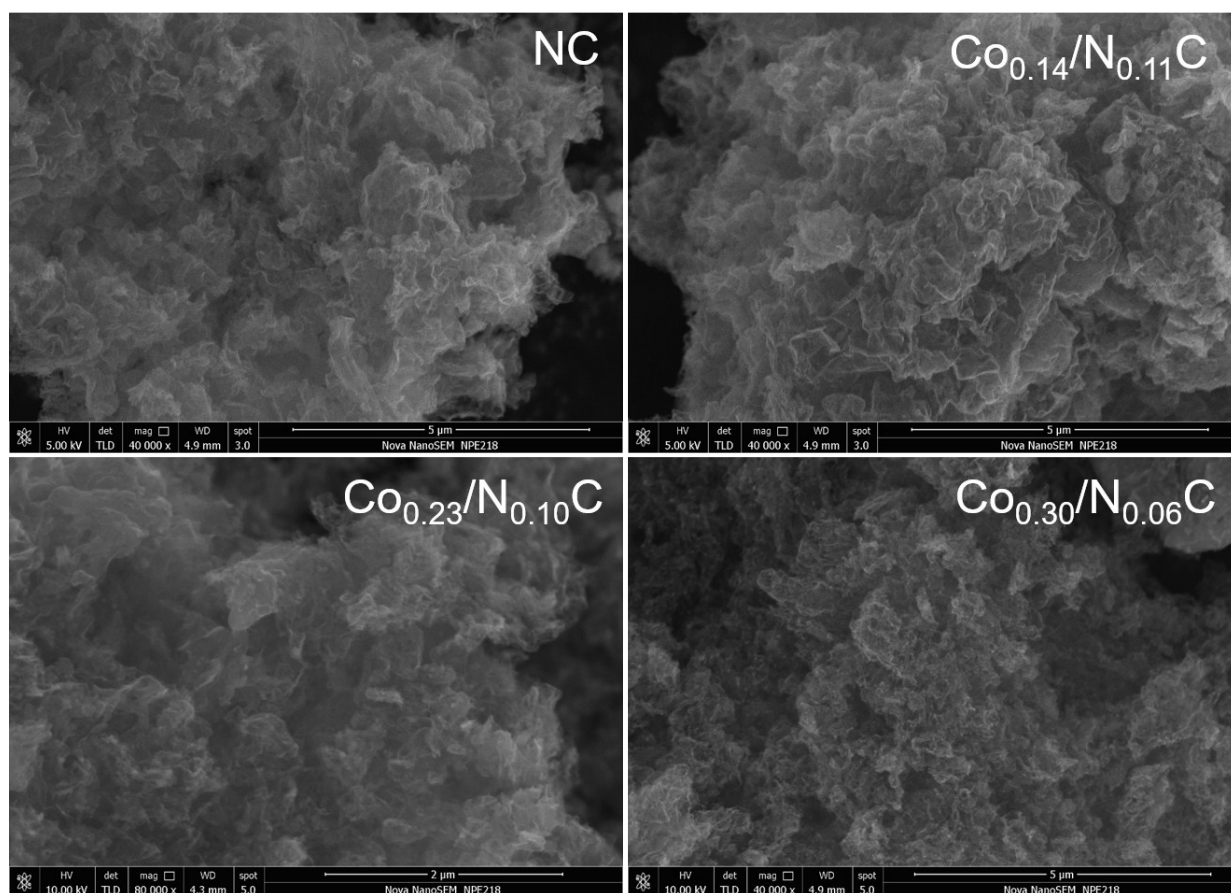
**Fig. S3**. Co K-edge EXAFS spectra and corresponding simulation curves for Co foil and Co/NC samples.
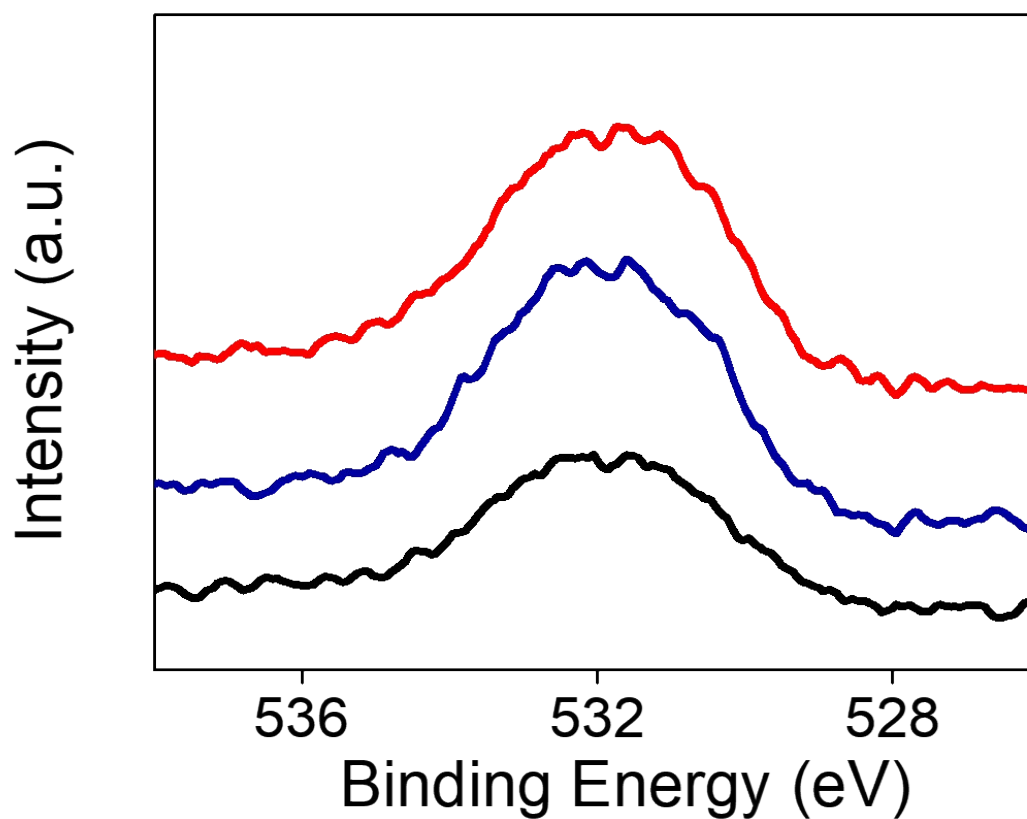
**Fig. S4**. High-resolution XPS O 1s spectra for $Co_{0.14}/N_{0.11}C$, $Co_{0.23}/N_{0.10}C$ or $Co_{0.3}/N_{0.06}C$. X-ray photoemission spectroscopy (XPS) O 1s peaks of typical $Co_x/N_yC$ samples centered at 532 eV excluded the presence of lattice oxygen with typical peak at 529 eV.

**Fig. S5.** Typical SEM images of NC, $Co_{0.14}/N_{0.11}C$, $Co_{0.23}/N_{0.10}C$ or $Co_{0.3}/N_{0.06}C$ samples. Two-dimensional carbonic foam was obseved in the controlled samples. It was noted that the introduction of metallic Co into N-doped carbon framework has not obvious effect on morphology of final products.
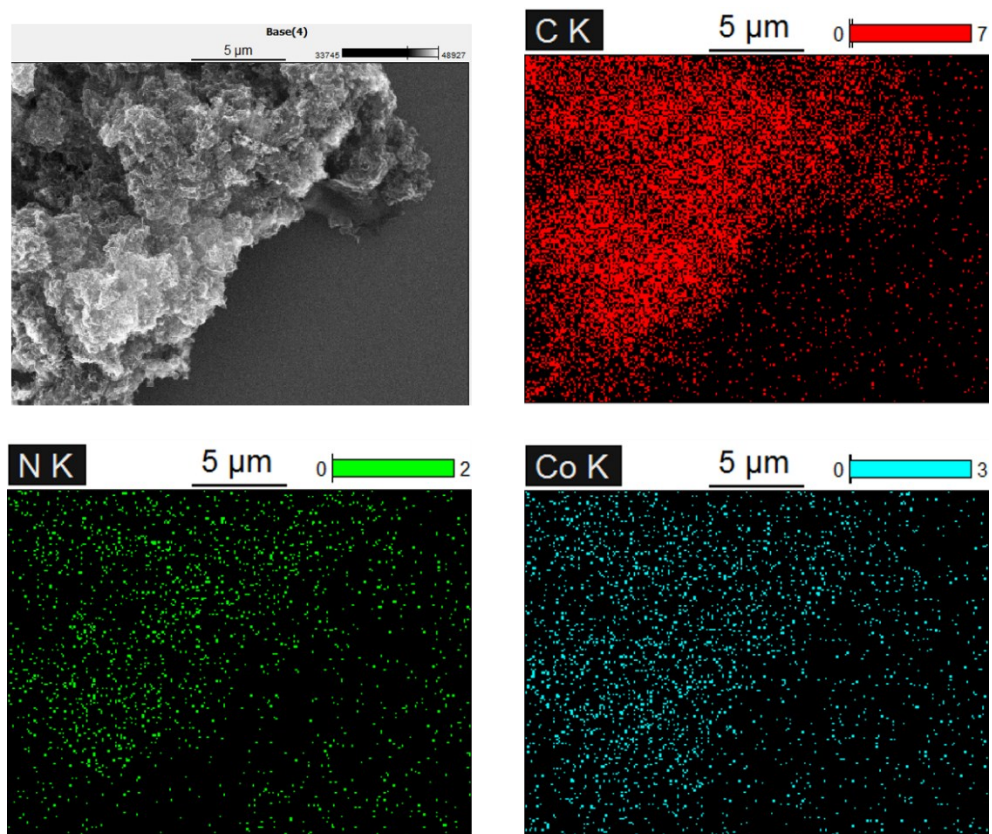
**Fig. S6.** Typical SEM image and elemental mapping images of $Co_{0.14}/N_{0.11}C$ sample.
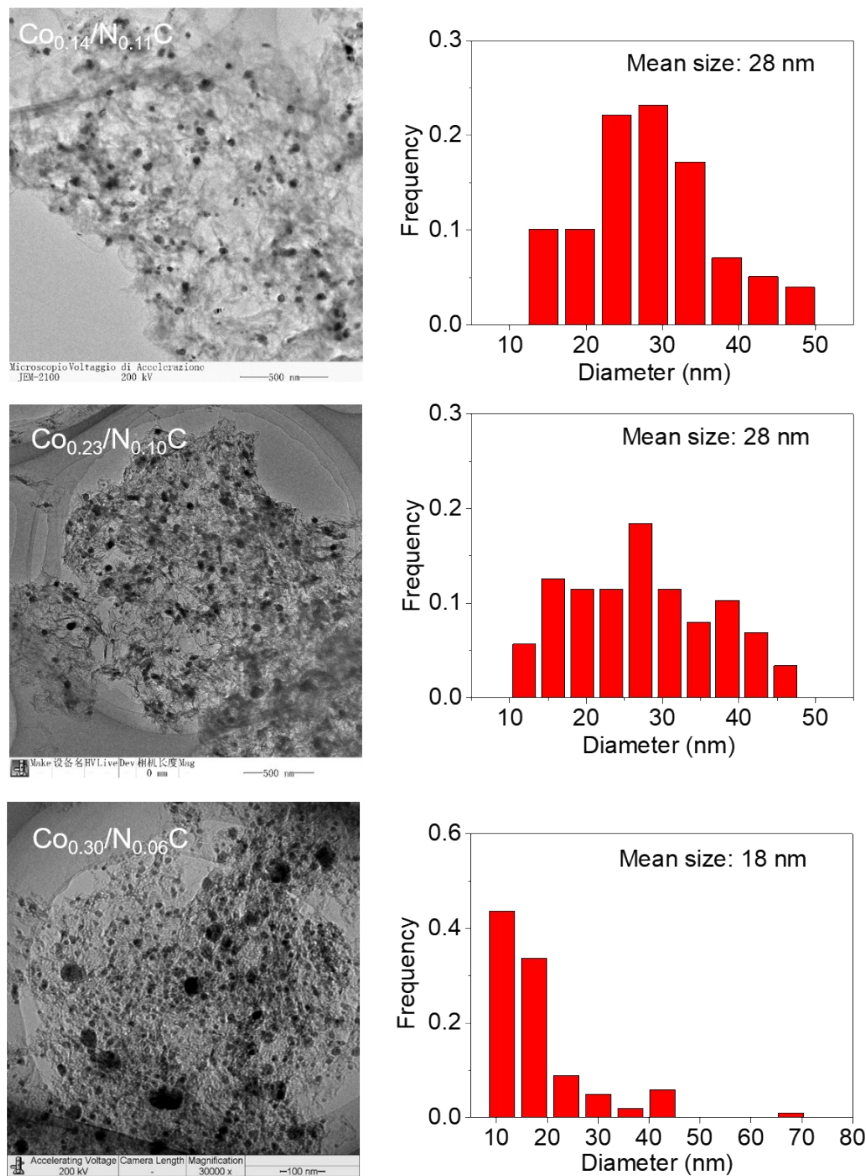
**Fig. S7**. Typical TEM images and the corresponding particle size distribution of $Co_{0.14}/N_{0.11}C$, $Co_{0.23}/N_{0.10}C$ or $Co_{0.3}/N_{0.06}C$ samples. The nitrogen thermal reaction of $Co^{2+}$-containing intermediates in the precursor with the nitrogen heteroatoms etches the carbon shells and makes the aggregation of released Co nanoparticles possible, resulting in a wide size distribution range and slightly decreased mean sizes of Co nanoparticles in Co/NC samples with higher Co contents.
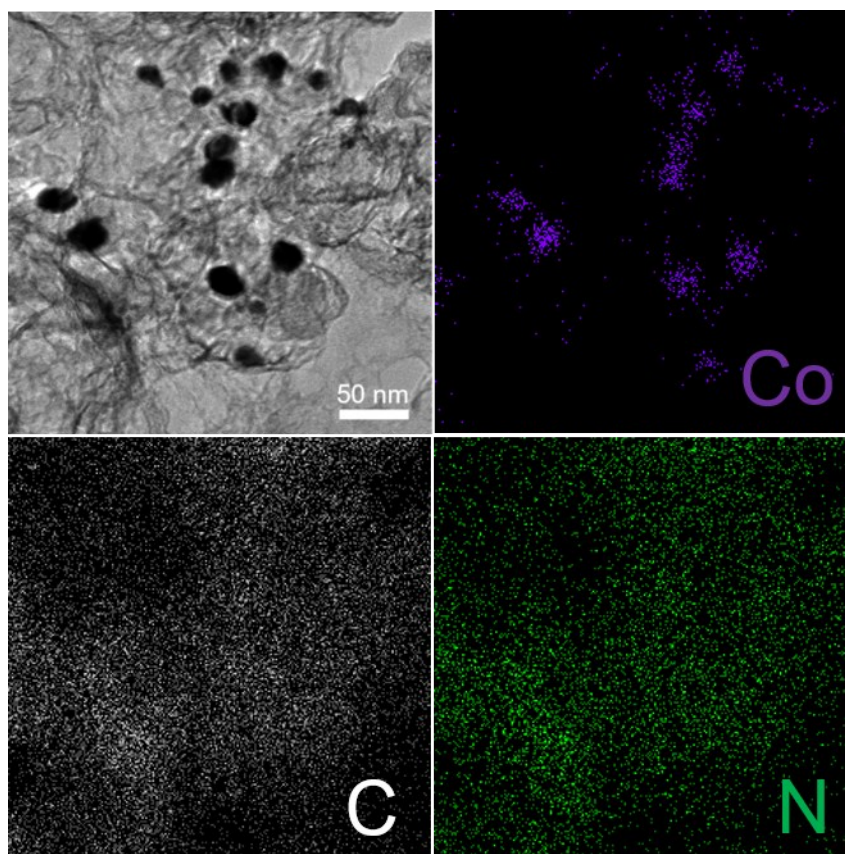
**Fig. S8**. Energy-filtered TEM elemental mapping of $Co_{0.14}/N_{0.11}C$. Well-defined Co nanoparticles with an average diameter of ~28 nm were observed to homogeneously spread over two-dimensional carbonic foam.
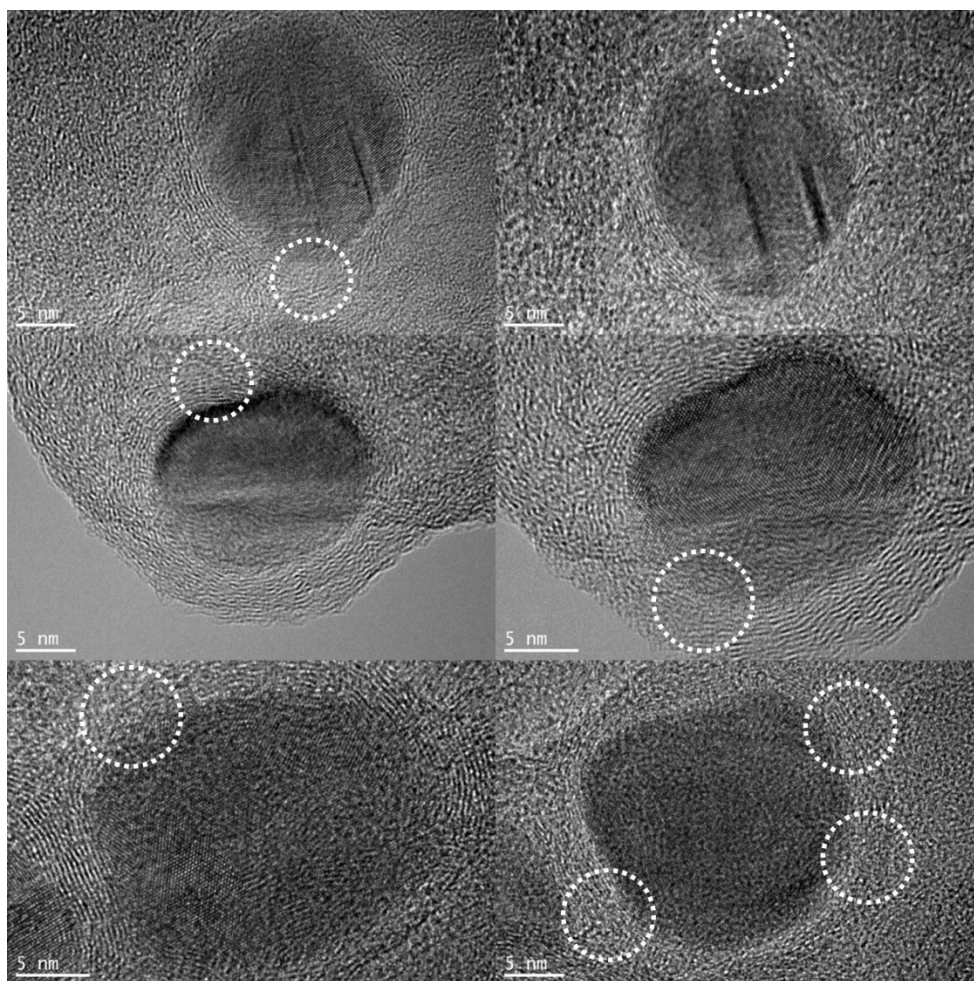
**Fig. S9**. HR-TEM images of $Co_{0.14}/N_{0.11}C$. Defective carbon shell coupled with Co nanoparticle was observed in HRTEM images of different areas, which facilitated mass transport of reactants to active metal sites. Considering the spherical shape of Co nanoparticles in all samples in this work, we excluded the possible effect of crystal facets on promoting their catalytic activity. Similar power XRD patterns and TEM morphologies with Co (111) as the most pronounced facets in all Co/NC samples (Figure 1b-c and S1, S7, S9-10) further indicate morphology of Co nanoparticle a negligible factor.
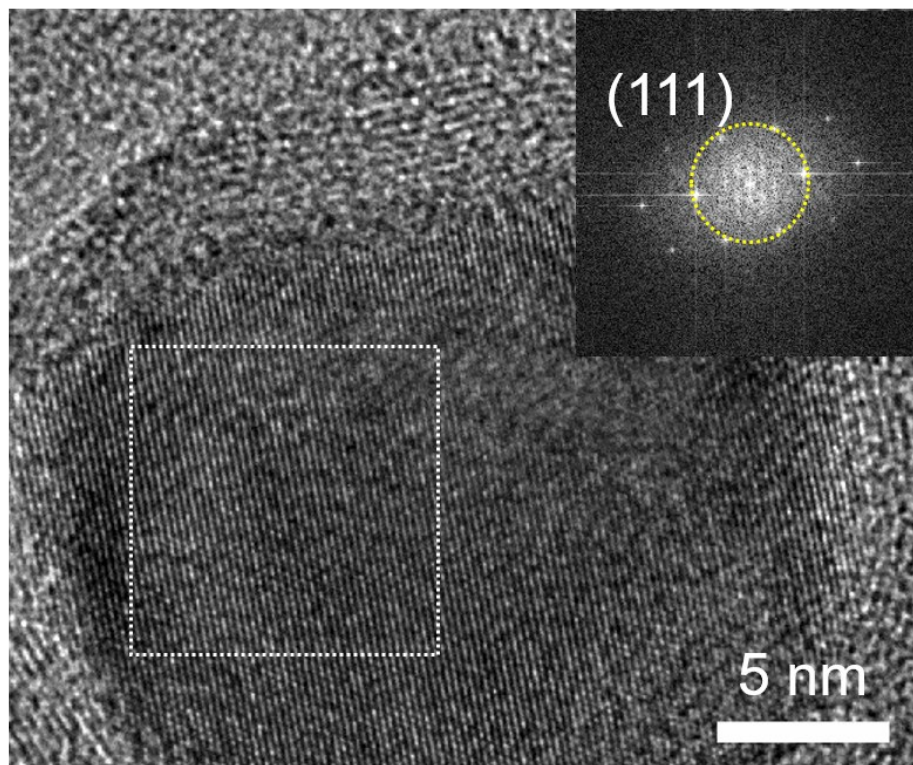
**Fig. S10**. HRTEM image and fast fourier transformation (FFT) pattern (inset) of $Co_{0.14}/N_{0.11}C$. The fast Fourier transform image revealed that the main exposed facet of Co nanoparticle is (111).
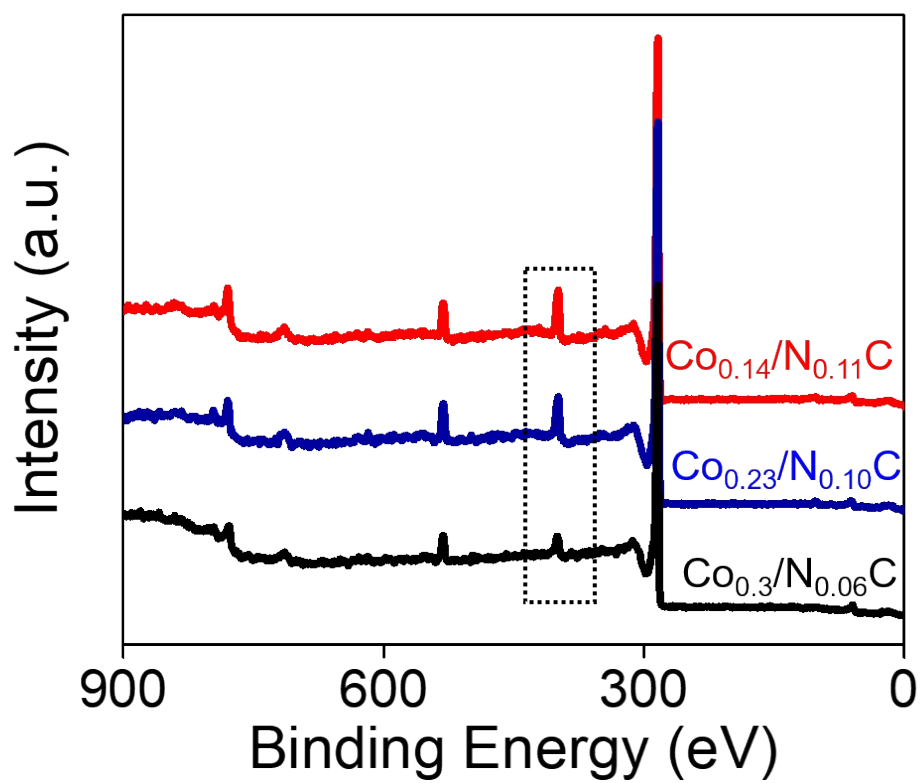
**Fig. S11**. XPS survey spectra of $Co_{0.14}/N_{0.11}C$, $Co_{0.23}/N_{0.10}C$ or $Co_{0.3}/N_{0.06}C$.
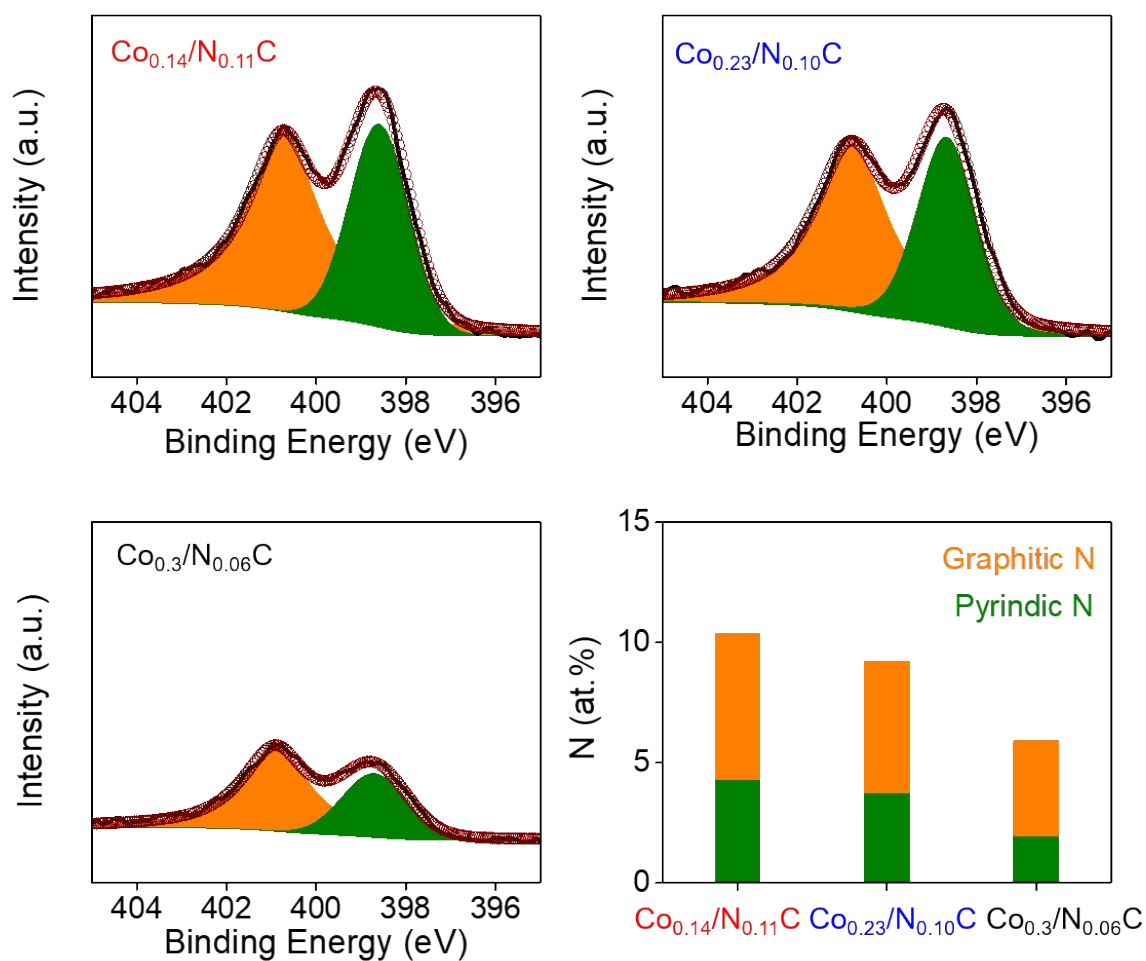
**Fig. S12**. High-resolution N 1s spectrum with the deconvoluted peak of graphitic N and pyridinic N peaks of $Co_{0.14}/N_{0.11}C$, $Co_{0.23}/N_{0.10}C$ or $Co_{0.3}/N_{0.06}C$. Both decreasing pyrindic and graphitic nitrogen content in carbon support for $Co_x/N_yC$ was ascribed to self-sacrificing reaction of the $Co^{2+}$-containing intermediates in the precursor to release gas N-containing compounds.[S4]
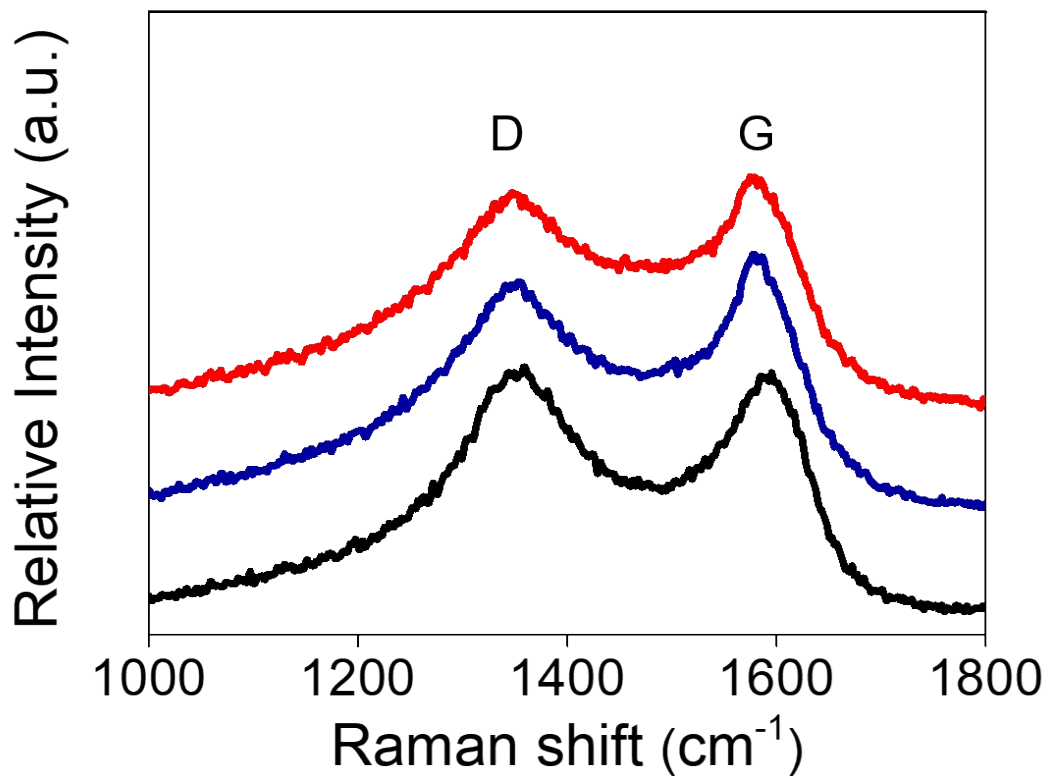
**Fig. S13**. Raman spectra of $Co_{0.14}/N_{0.11}C$, $Co_{0.23}/N_{0.10}C$ or $Co_{0.3}/N_{0.06}C$ samples. The intensity ratio of D and G band ($I_D/I_G$) for $Co_{0.14}/N_{0.11}C$, $Co_{0.23}/N_{0.10}C$ or $Co_{0.3}/N_{0.06}C$ samples is 0.91, 0.94 and 1.03 respectively. The high Co content of Co/NC sample with higher value of $I_D/I_G$ shown more defects in carbon shell, further revealing intensive reaction bewteen metal nanoparticle and carbon shell.
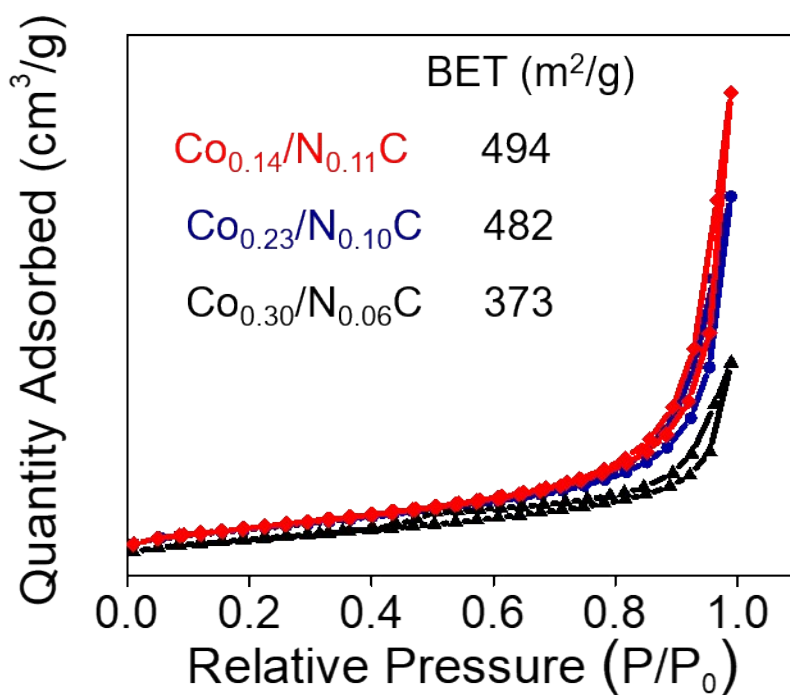
**Fig. S14**. $N_2$ adsorption and desorption isotherm curves of $Co_{0.14}/N_{0.11}C$, $Co_{0.23}/N_{0.10}C$ or $Co_{0.3}/N_{0.06}C$. Integrating Co particles and carbonic support still enabled catalyst to be a relatively high surface area value, which ensured the sufficient contact of metal active sites and reactants.
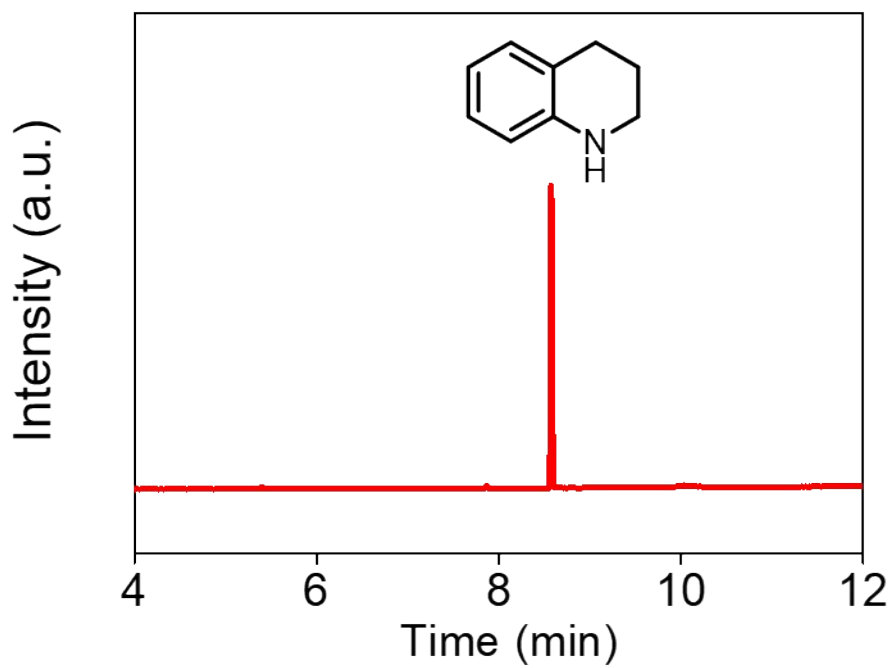
**Fig. S15**. GC-MS spectra of products after hydrogenaion of quinoline under solvent-free condition over $Co_{0.14}/N_{0.11}C$ for 57 h.
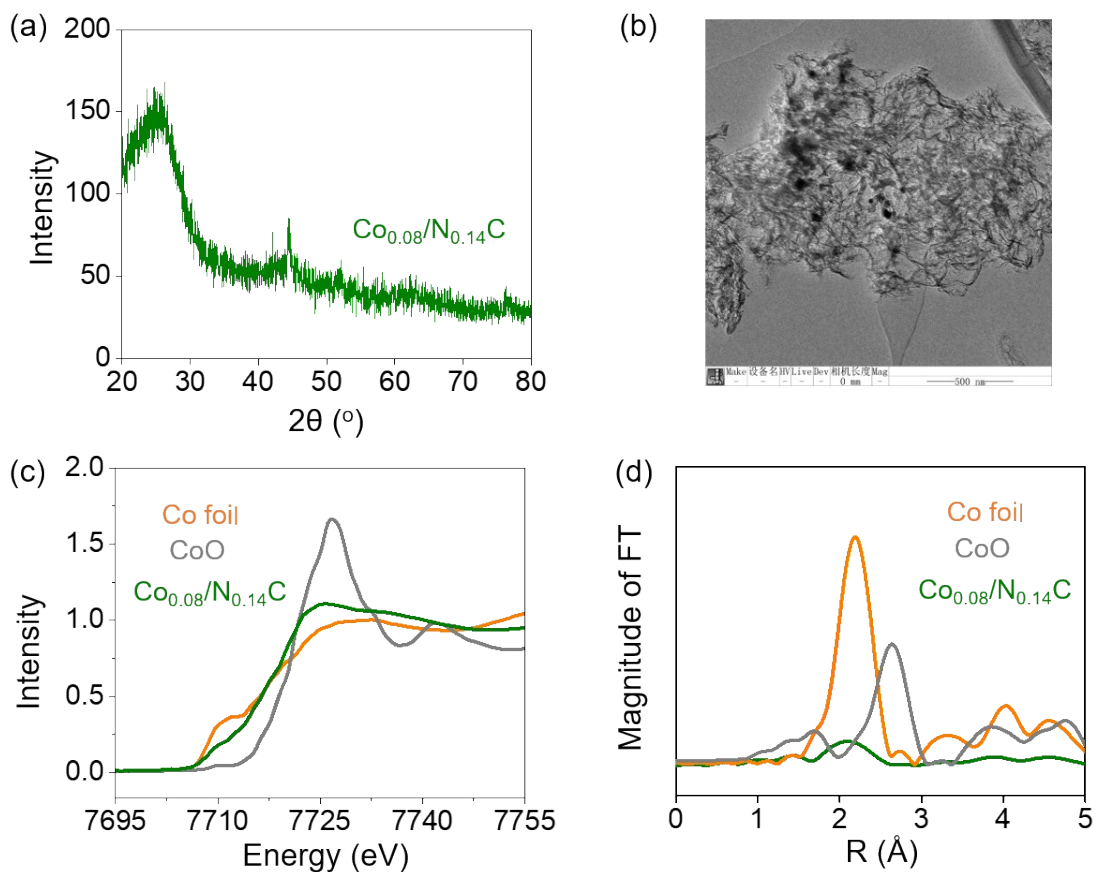
**Fig. S16**. (a) The XRD profile, (b) TEM image, (c) normalized XANES spectra and (d) the corresponding Fourier-transformed EXAFS spectra of $Co_{0.08}/N_{0.14}C$ sample. The $Co_{0.08}/N_{0.14}C$ with higher nitrogen dopant in carbonic support shown the silmilar structure of supported metallic Co nanoparticle in two-dimension carbon matrix with bench-mark $Co_{0.14}/N_{0.11}C$. Hence, the lower activity of $Co_{0.08}/N_{0.14}C$ for hydrogenation reaction was ascribed to insufficient amount of exposed rectifying interface of Co and N-doped carbon support.
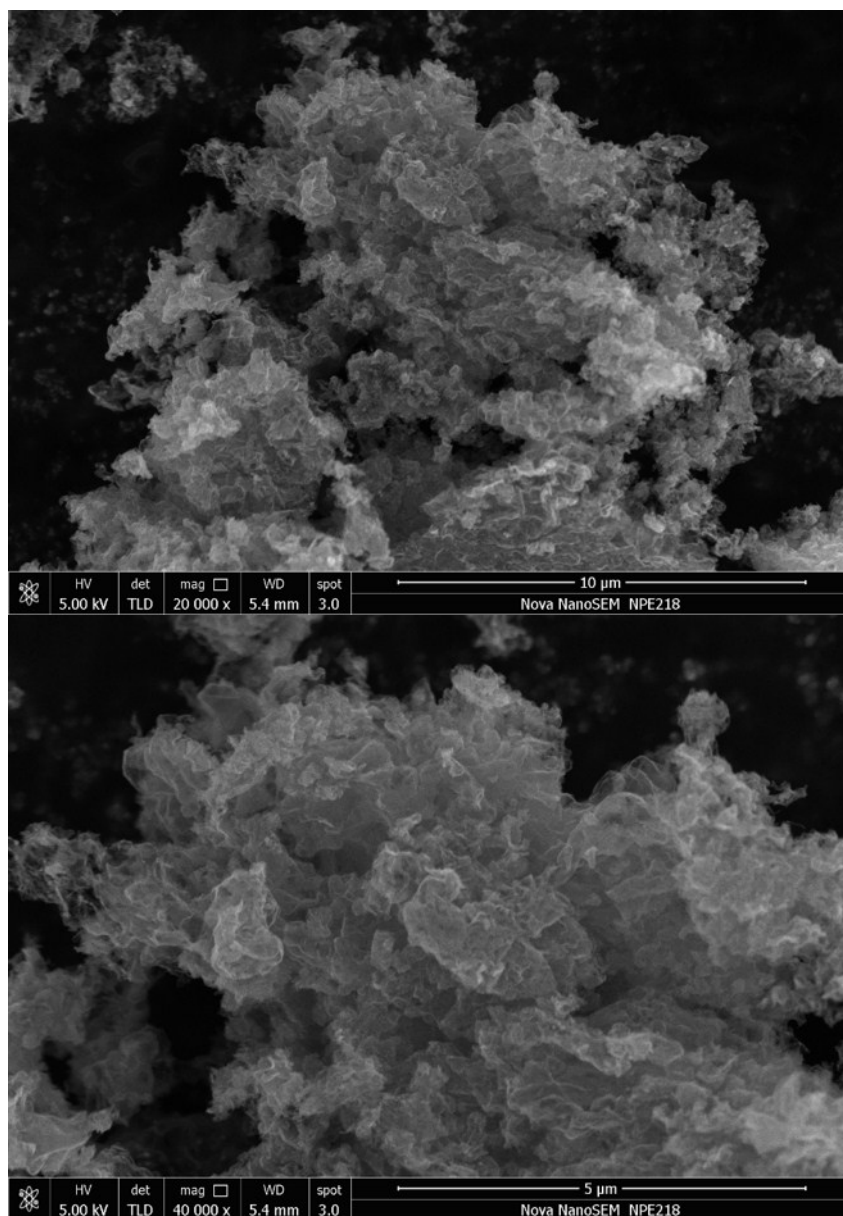
**Fig. S17**. SEM images of $Co_{0.14}/N_{0.11}C\text{-}H^+$ sample. The morphology of $Co_{0.14}/N_{0.11}C$ after mild acid treatment maintaned well.

**Co_{0.14}/N_{0.11}C**

Energy (Ha) = -3504.7108725

Energy (Ha) = -3504.7564026

Energy (Ha) = -3504.7265460

Energy (Ha) = -3504.7229529

**Co_{0.23}/N_{0.10}C**

Energy (Ha) = -3471.4436754

Energy (Ha) = -3471.4626769

Energy (Ha) = -3471.4579399

Energy (Ha) = -3471.4578642

**Co_{0.3}/N_{0.06}C**

Energy (Ha) = -3438.2532614

Energy (Ha) = -3438.2540686

Energy (Ha) = -3438.2583324

Energy (Ha) = -3438.2512905
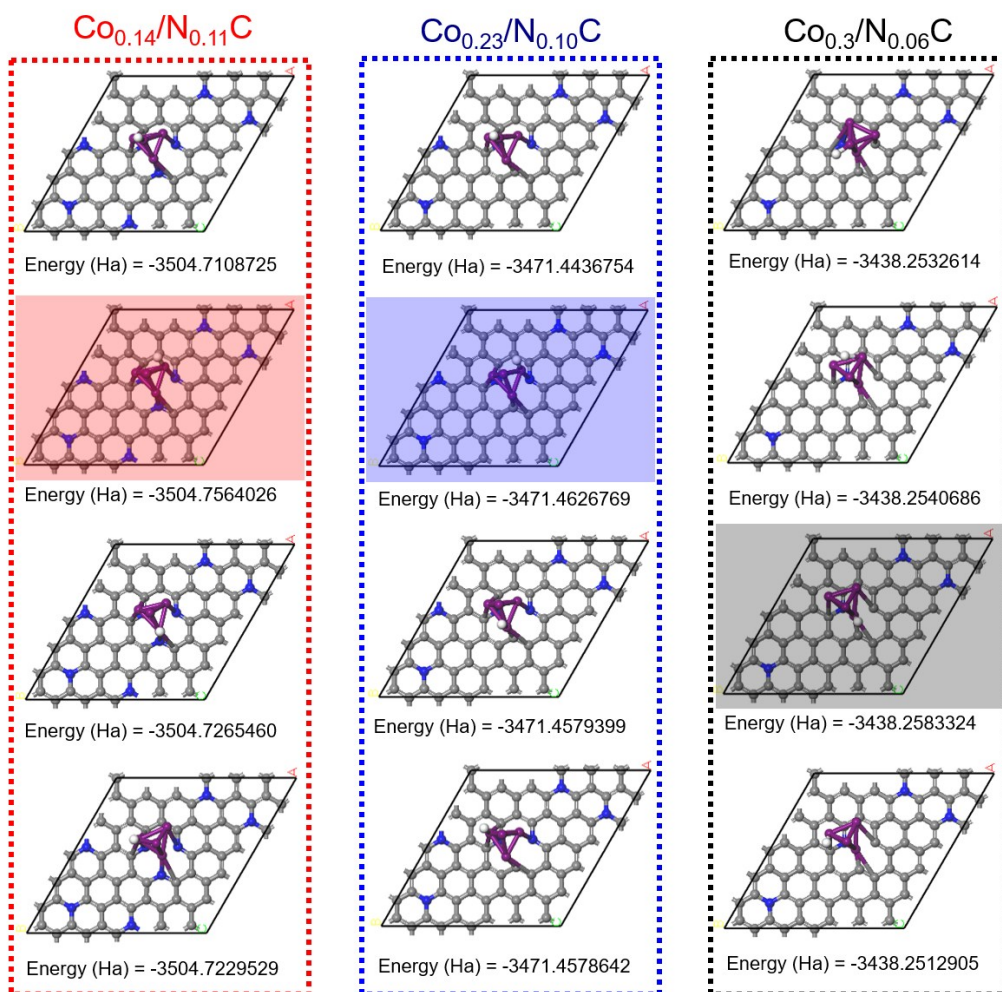
**Fig. S18**. Typical adsorption models of H atom on the surface of $Co_{0.14}/N_{0.11}C$, $Co_{0.23}/N_{0.10}C$ or $Co_{0.3}/N_{0.06}C$. Different adsorption configurations was stimulated for $Co_{0.14}/N_{0.11}C$, $Co_{0.23}/N_{0.10}C$ or $Co_{0.3}/N_{0.06}C$. We selected lowest total energy of configurations as final model respectively.
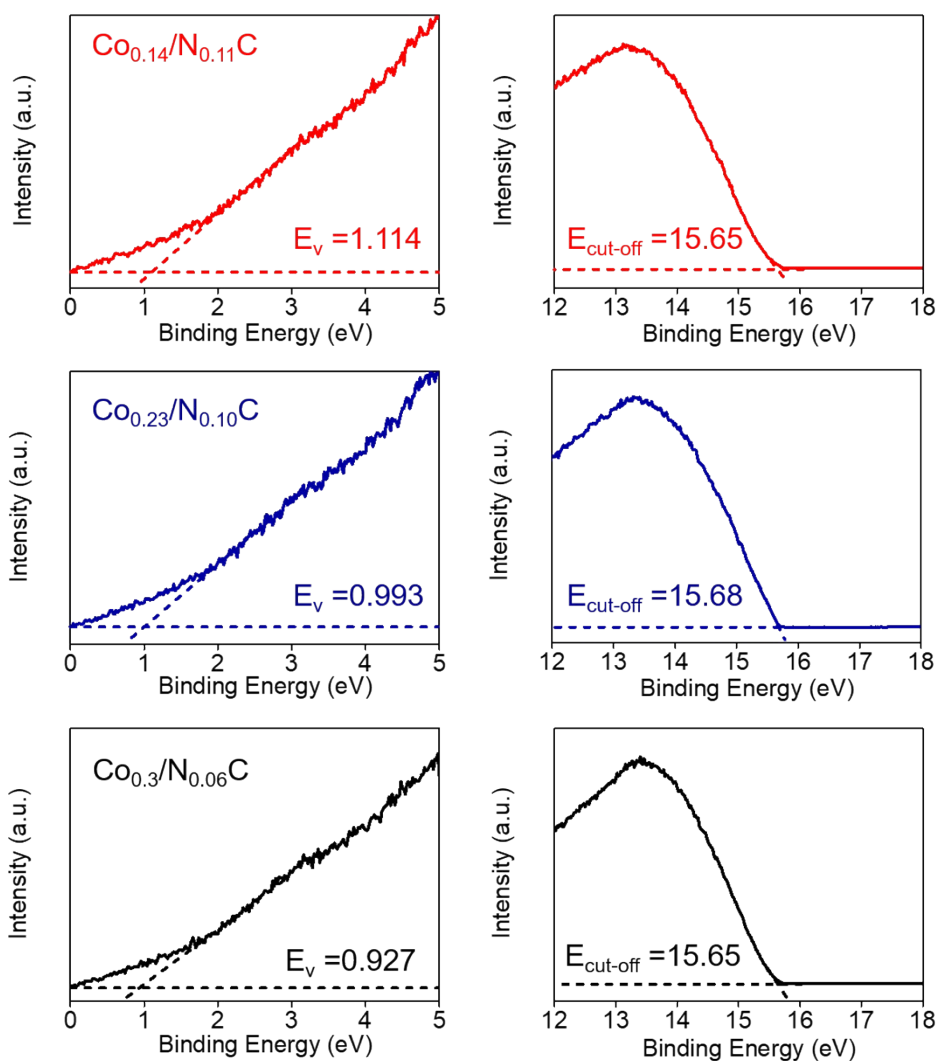
**Fig. S19**. UPS spectra in onset ($E_V$) and secondary electron cut-off ($E_{cut-off}$) energy boundary for Co/NC catalysts. The work function of calculated as following equation, $\Phi=21.22$ eV -($E_{cut-off}$ - $E_V$) was 6.684 eV, 6.533 eV, 6.497 eV for $Co_{0.14}/N_{0.11}C$, $Co_{0.23}/N_{0.10}C$ or $Co_{0.3}/N_{0.06}C$ respectively. As reflected as lower valence band position of Co/NC, enlarged Schottky barrier further enhanced electron transfer from metal to carbonic "electron trap" via increasing nitrogen doped content in carbon support from $Co_{0.14}/N_{0.11}C$ via $Co_{0.23}/N_{0.10}C$ to $Co_{0.3}/N_{0.06}C$.
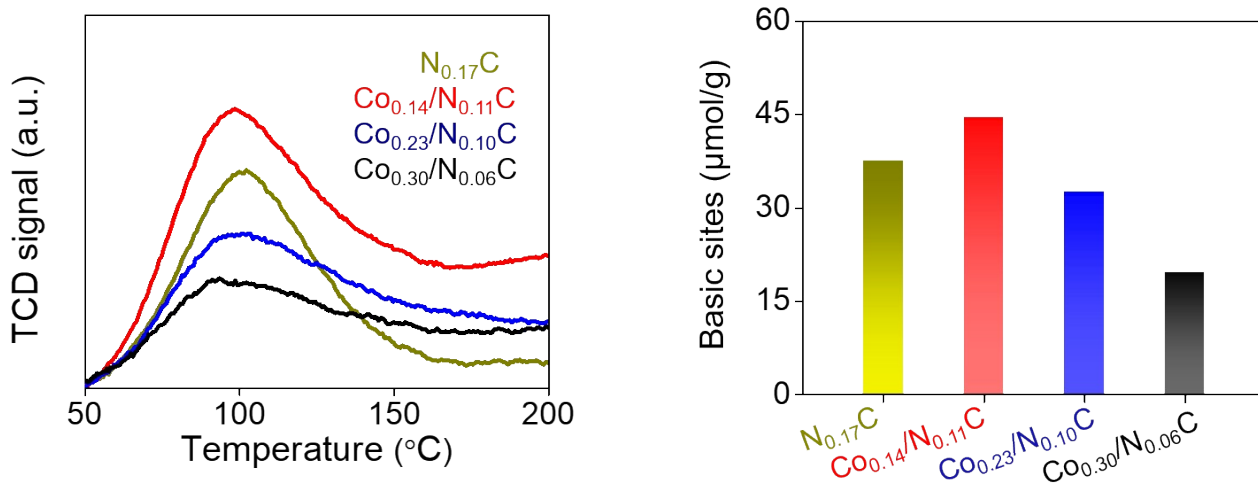
**Fig. S20**. $CO_2$-TPD profiles and the amounts of basic sites for NC, $Co_{0.14}/N_{0.11}C$, $Co_{0.23}/N_{0.10}C$ or $Co_{0.3}/N_{0.06}C$. The increased electron enrichment of carbonic support was revealed by the fact of higher desorption peak of $Co_{0.14}/N_{0.11}C$ than that for $Co_{0.23}/N_{0.10}C$ and $Co_{0.3}/N_{0.06}C$ further speaking for the key role of rectifying contact bewteen Co and NC on adjusting electronic propoerty of carbonic support.
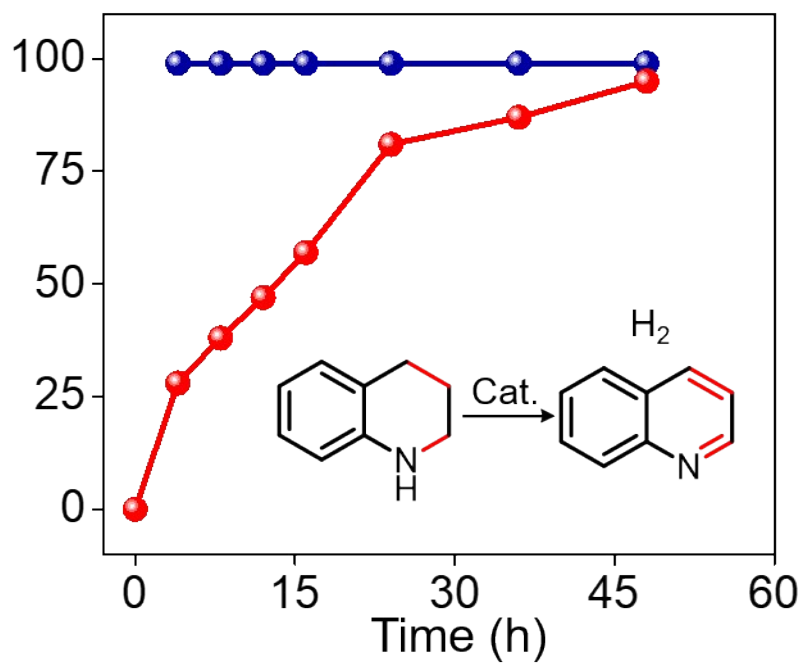
**Fig. S21**. Conversion and selectivity to 1, 2, 3, 4-tetrahydroquinoline for hydrogenation of quinoline over $Co_{0.14}/N_{0.11}C$ at different time.
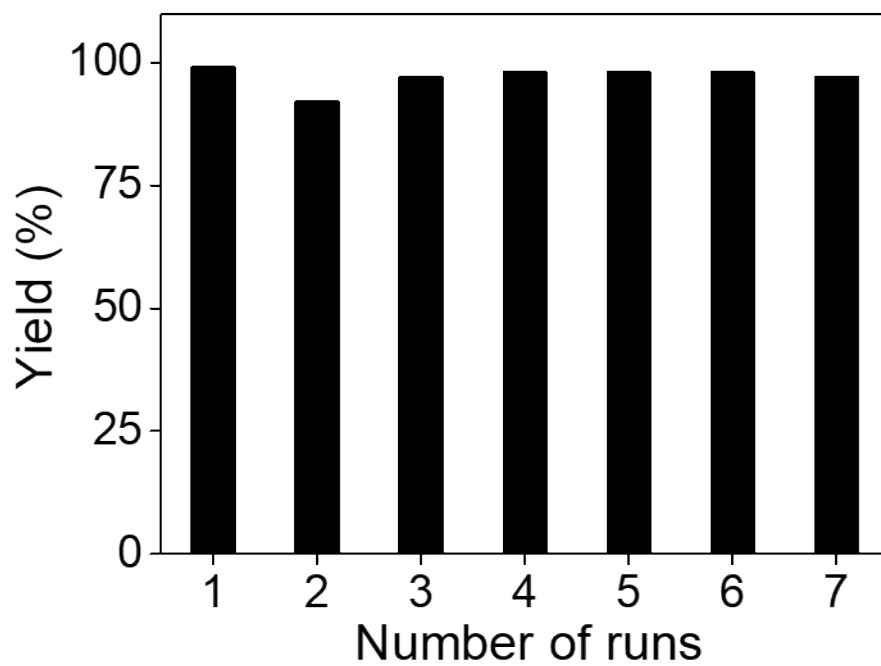
**Fig. S22**. Recycle experiment for hydrogenation of quinoline over $Co_{0.14}/N_{0.11}C$. Reaction condition: 0.1 mmol of quinoline, 10 ml of toluene, 100 mg of catalyst, 120 $^oC$, 2 h, 30 bar of hydorgen gas.
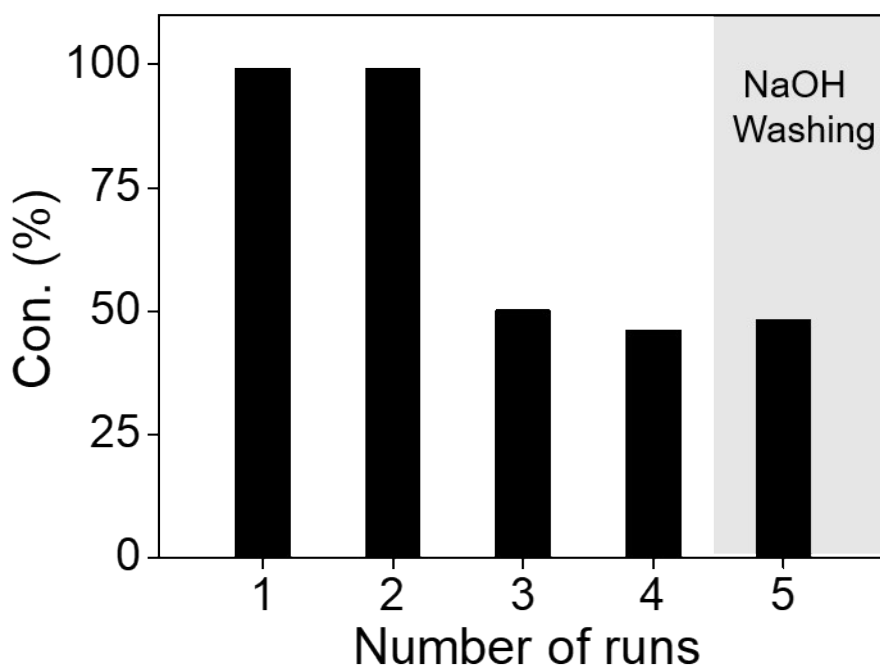
**Fig. S23**. Recycling of 1, 2, 3, 4-tetrahydroquinoline dehydrogenation reaction. The aggregation of Co/NC catalyst after recycling test is mainly responsible for the attenuation of dehydrogenative activity. There is no obvious improvement on reactivity via following base-washing treatment for catalyst, which indicated that an important role of electron-rich N-doped carbon support on efficiently catalyzing tetrahydroquinoline dehydrogenation reaction.
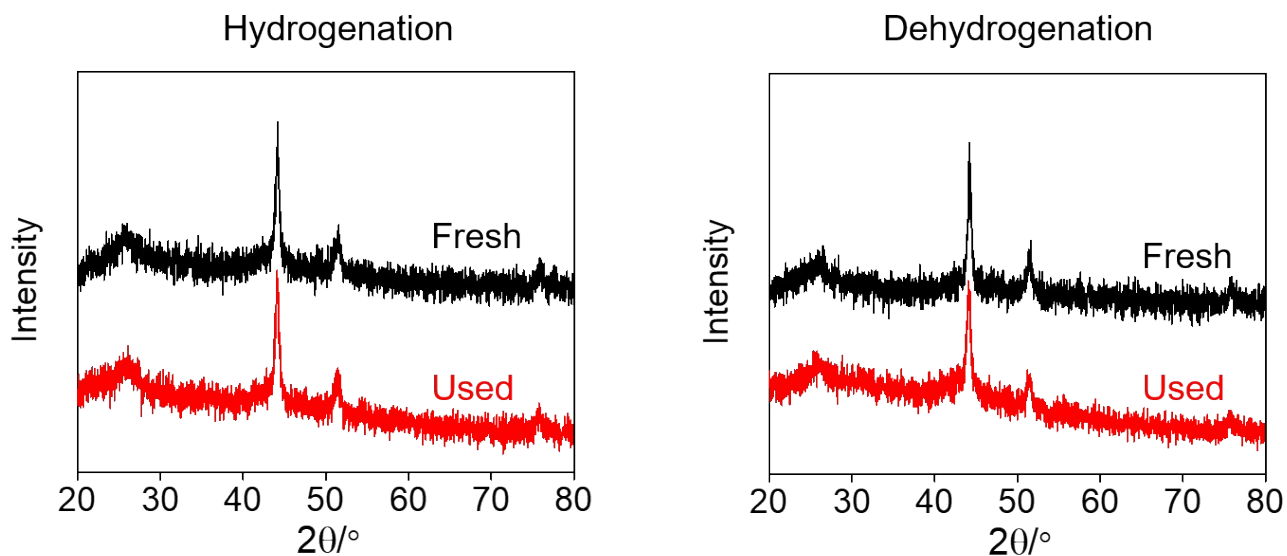
**Fig. S24.** Power XRD pattern of fresh and used catalyst after hydrogenation and dehydrogenation recycling test. The metallic cobalt feature did not changed obviously, which indicated the robustness of rectifying contact of Co nanoparticle and N-doped carbon support.

**Table S1.** Structure parameters derived from the EXAFS simulation of Co foil and Co/NC samples.

| Sample | Path | N | R/Å | $\Delta E_0$ (eV) | $\Delta\sigma^2$ (Å$^2$) | R-factor |
|--------|------|---|-----|-------------------|--------------------------|----------|
| Co foil | Co-Co | 12 | 2.49 | 6.79 | 0.006 | 0.002 |
| $Co_{0.14}/N_{0.11}C$ | Co-Co | 8.2 | 2.49 | 6.76 | 0.007 | 0.004 |
| $Co_{0.23}/N_{0.10}C$ | Co-Co | 10.4 | 2.50 | 7.07 | 0.007 | 0.003 |
| $Co_{0.3}/N_{0.06}C$ | Co-Co | 9.7 | 2.50 | 7.08 | 0.007 | 0.005 |

N is the coordination number; R is interatomic distance; $\Delta E_0$ is edge-energy shift; $\Delta\sigma^2$ is Debye-Waller factor; The data range for data fitting in k-space ($\Delta k$) and R space ($\Delta R$) are 3-14 and 1-3 Å, respectively.

**Table S2.** Elemental composition of catalysts.

| sample | Co (wt.%) by ICP | N (wt.%) by XPS | C (wt.%) by XPS |
|---|---|---|---|
| $N_{0.17}C$ | - | 17 | 81 |
| $Co_{0.08}/N_{0.14}C$ | 8 | 14 | 71 |
| $Co_{0.14}/N_{0.11}C$ | 14 | 11 | 74 |
| $Co_{0.23}/N_{0.10}C$ | 23 | 10 | 76 |
| $Co_{0.3}/N_{0.06}C$ | 30 | 6.0 | 81 |
| $Co_{0.08}/N_{0.14}C-H^+$ | 5.1 | - | - |
| $Co_{0.14}/N_{0.11}C-H^+$ | 9.5 | - | - |
| $Co_{0.23}/N_{0.10}C-H^+$ | 9.0 | - | - |
| $Co_{0.3}/N_{0.06}C-H^+$ | 5.5 | - | - |

**Table S3.** The hydrogenation performance for $Co_x/N_yC$ samples.
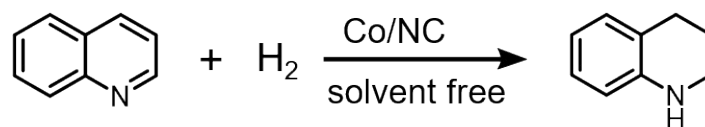


| Entry | Catalyst | T (°C) | H₂ pressure (bar) | Time (h) | Mass (mg) | Con. (%) | TOF (h⁻¹) |
|-------|----------|--------|-------------------|----------|-----------|----------|-----------|
| 1 | No catalyst | 120 | 30 | 4 h | -- | -- | -- |
| 2 | $N_{0.17}C$ | 120 | 30 | 4 h | -- | -- | -- |
| 3 | $Co_{0.08}/N_{0.14}C$ | 120 | 30 | 4 h | 52 | 8.3 | 13 |
| 4 | $Co_{0.14}/N_{0.11}C$ | 120 | 30 | 4 h | 30 | 22 | 34 |
| 5 | $Co_{0.23}/N_{0.10}C$ | 120 | 30 | 4 h | 18 | 14.6 | 23 |
| 6 | $Co_{0.3}/N_{0.06}C$ | 120 | 30 | 4 h | 14 | 8.7 | 13 |

**Hydrogenation condition:** 44 mmol of quinoline, 0.16 mol % Co catalyst, 120 °C.

**Table S4.** $Co_{0.14}/N_{0.11}C$-catalyzed hydrogenation of quinoline at different interval.
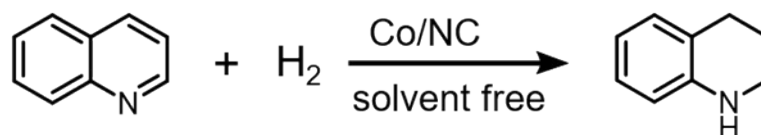


| Catalyst | T (°C) | H₂ pressure (bar) | Time (h) | Con. (%) | TOF (h⁻¹) | TON |
|---|---|---|---|---|---|---|
| | 120 | 30 | 4 h | 22 | 34 | 135 |
| | 120 | 30 | 8 h | 41 | 31 | 253 |
| | 120 | 30 | 12 h | 56 | 28 | 345 |
| | 120 | 30 | 17 h | 69 | 25 | 426 |
| $Co_{0.14}/N_{0.11}C$ | 120 | 30 | 22 h | 81 | 22 | 500 |
| | 120 | 30 | 27 h | 87 | 20 | 537 |
| | 120 | 30 | 37 h | 95 | 16 | 586 |
| | 120 | 30 | 47 h | 97 | 13 | 599 |
| | 120 | 30 | 57 h | 99 | 11 | 611 |

The TON value was calculated in the format of mol $_{1, 2, 3, 4\text{-tetrahydroquinoline}}$ $mol_{metal}^{-1}$. The amount of metal is based on the moles of metal components involved.

**Table S5.** $Co_{0.14}/N_{0.11}C$-catalyzed hydrogenation reaction under solvent condition.
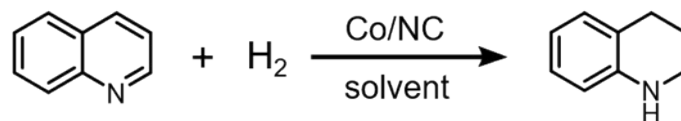


| Entry | Catalyst | T (°C) | Time (h) | Con. (%) | Carbon balance (%) |
|-------|----------|--------|----------|----------|--------------------|
| 1 | $Co_{0.14}/N_{0.11}C$ | 120 | 4 | 47 | 98 |
| 2 | $Co_{0.14}/N_{0.11}C$ | 120 | 8 | 89 | - |
| 3 | $Co_{0.14}/N_{0.11}C$ | 120 | 12 | 94 | - |
| 4 | $Co_{0.14}/N_{0.11}C$ | 120 | 16 | 99 | 95 |
| 5 | $Co_{0.14}/N_{0.11}C-H^+$ (HCl) | 120 | 16 | 22 | - |
| 6 | $Co_{0.14}/N_{0.11}C-H^+$ (HNO$_3$) | 120 | 16 | 10 | - |

**Hydrogenation condition:** 0.5 mmol of quinoline, 20 mg of catalyst, 120 °C and 5 bar of $H_2$.

$Cl^-$ may be a poison to reduce the hydrogenation activity. In order to eliminate the role of $Cl^-$ as poison to metal sites on hydrogenation activity, we also used $HNO_3$ (7.5 M) to etch the Co nanoparticles in $Co_{0.14}/N_{0.11}C$ under mild condition. The as-obtained $Co_{0.14}/N_{0.11}C-H^+$ ($HNO_3$) also significantly reduced the hydrogenation activity achieving a lower conversion (10 %, Entry 6 of Table S5), excluding possible effect of $Cl^-$ on poisoning active centers.

**Table S6.** Optimized results of hydrogenation reaction condition.
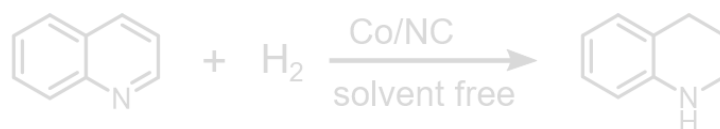


| Catalyst | T (°C) | H₂ pressure (bar) | Time (h) | Mass (mg) | Con. (%) | TOF (h⁻¹) |
|---|---|---|---|---|---|---|
| $Co_{0.14}/N_{0.11}C$ | 120 | 30 | 4 h | 5 | 2 | 19 |
| $Co_{0.14}/N_{0.11}C$ | 120 | 30 | 4 h | 10 | 4 | 19 |
| $Co_{0.14}/N_{0.11}C$ | 120 | 30 | 4 h | 20 | 11 | 25 |
| $Co_{0.14}/N_{0.11}C$ | 120 | 30 | 4 h | 30 | 22 | 34 |
| $Co_{0.14}/N_{0.11}C$ | 120 | 30 | 4 h | 40 | 24 | 28 |

TOF value was calculated by the following equation:

TOF value = (Yielded mol 1, 2, 3, 4-tetrahydroquinoline)/(Total mol metal)×(Reaction time)

(Yielded mol 1, 2, 3, 4-tetrahydroquinoline) = (Initial mol of quinoline)×(Conversion of quinoline after reaction time)× (Selectivity to 1, 2, 3, 4-tetrahydroquinoline)

(Total mol metal) = (Weight of catalyst)×(Mass concentration of Co)/(Molar mass of Co)

**Table S7.** Summary of results for hydrogenation of quinoline over reported Co-based catalysts.
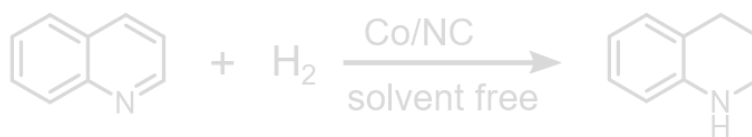


| Catalyst | Condition | TOF (h$^{-1}$) | Reference |
|---|---|---|---|
| Co$_{0.14}$/N$_{0.11}$C | 5 bar H$_2$, Toluene, 120°C, 8h | 1.06 | This work |
| Co$_{0.14}$/N$_{0.11}$C | 30 bar H$_2$, solvent-free, 120°C, 4h | 34 | This work |
| ISAS-Co/OPNC | 15 bar H$_2$, Toluene, 120°C, 12h | 2.78 | S5 |
| CoO$_X$@NC | 30 bar H$_2$, methenol, 120°C, 3h | 6.5 | S6 |
| Co$_3$O$_4$−Co/NGr@α-Al$_2$O$_3$ | 5 bar H$_2$, Toluene, 120°C, 48h | 0.26 | S7 |
| Co$_3$O$_4$−Co/NGr@α-Al$_2$O$_3$ | 20 bar H$_2$, Toluene, 120°C, 48h | 0.47 | S7 |
| Homogeneous Co Pincer | 10 bar H$_2$, THF, 120°C, 48h | 0.2 | S8 |
| Homogeneous Co complex | 10 bar H$_2$, THF, 60°C, 15h | 2.2 | S9 |

**Table S8.** Activity toward dehydrogenation of 1, 2, 3, 4-tetrahydroquinoline over different catalysts.
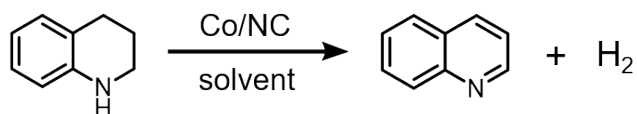


| Entry | Catalyst | T (°C) | Time (h) | Con. (%) |
|-------|----------|--------|----------|----------|
| 1 | No cat. | 160 | 12 | 3.7 |
| 2 | NC | 160 | 12 | 32 |
| 3 | $Co_{0.14}/N_{0.11}C$ | 160 | 12 | 47 |
| 4 | $Co_{0.23}/N_{0.10}C$ | 160 | 12 | 40 |
| 5 | $Co_{0.3}/N_{0.06}C$ | 160 | 12 | 35 |

**Dehydrogenation condition:** 0.5 mmol of 1, 2, 3, 4-tetrahydroquinoline, 10 mL of toluene, 100 mg of catalyst, 160 °C, 12 h and 30 bar of Ar.

**Table S9.** $Co_{0.14}/N_{0.11}C$-catalyzed dehydrogenation of 1, 2, 3, 4-tetrahydroquinoline at different reaction time.



| Entry | Catalyst | T (°C) | Time (h) | Con. (%) |
|-------|----------|--------|----------|----------|
| 1 | $Co_{0.14}/N_{0.11}C$ | 160 | 4 | 28 |
| 2 | $Co_{0.14}/N_{0.11}C$ | 160 | 8 | 38 |
| 3 | $Co_{0.14}/N_{0.11}C$ | 160 | 12 | 47 |
| 4 | $Co_{0.14}/N_{0.11}C$ | 160 | 16 | 57 |
| 5 | $Co_{0.14}/N_{0.11}C$ | 160 | 24 | 81 |
| 6 | $Co_{0.14}/N_{0.11}C$ | 160 | 36 | 87 |
| 7 | $Co_{0.14}/N_{0.11}C$ | 160 | 48 | 95 |

**Dehydrogenation condition:** 0.5 mmol of 1, 2, 3, 4-tetrahydroquinoline, 10 mL of toluene, 100 mg of catalyst, 160 °C and 30 bar of Ar.

**Table S10.** Catalystic peformance of $Co_{0.14}/N_{0.11}C$ for reversible $H_2$ uptake and release.
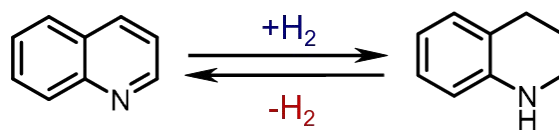


| Catalyst | T (°C) | gas pressure | Time (h) | Con. (%) |
|----------|--------|--------------|----------|----------|
| $Co_{0.14}/N_{0.11}C$ | 160 | 30 bar Ar | 8 h | 99 |
| $Co_{0.14}/N_{0.11}C$ | 120 | 5 bar $H_2$ | 4 h | 99 |
| $Co_{0.14}/N_{0.11}C$ | 160 | 30 bar Ar | 48 h | 99 |
| $Co_{0.14}/N_{0.11}C$ | 120 | 5 bar $H_2$ | 4 h | 99 |

**Hydrogenation-dehydrogenation condition:** 0.1 mmol of substrate, 10 ml of toluene, 100 mg of $Co_{0.14}/N_{0.11}C$.

**Table S11.** Summary of results for reversible hydrogenation-dehydrogenation reaction activity of Heteroarene over reported catalysts.
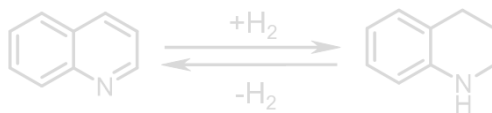


| Catalyst | Hydrogenation Condition | Hydrogenation Conversion | Dehydrogenation Condition | Dehydrogenation Conversion | Reference |
|---|---|---|---|---|---|
| $Co_{0.14}/N_{0.11}C$ | 5 bar $H_2$, Toluene, 120°C, 4 h | 99 | 30 bar Ar, Toluene, 160°C, 8 h | 99 | This work |
| ISAS-Co/OPNC | 15 bar $H_2$, Toluene, 120°C, 12 h | 99 | Ar, Mesitylene, 120°C, 8 h | 99 | S5 |
| Ni–Si/NiO–SiO$_2$@SiO$_2$ | 50 bar $H_2$, triglyme, 120°C, 16 h | 100 | Ar, triglyme, 200°C, 24 h | 57 | S10 |
| Cu/TiO$_2$ | 1 bar $H_2$, mesitylene, 150°C, 6 h | 95 | Ar, mesitylene, 150°C, 16 h | 99 | S11 |

**Table S12.** Recycling result of dehydrogenation reaction over $Co_{0.14}/N_{0.11}C$.



| Entry | Catalyst | T (°C) | Time (h) | Con. (%) |
|-------|----------|--------|----------|----------|
| 1 | $Co_{0.14}/N_{0.11}C$ (1 cycle) | 160 | 8 | 99 |
| 2 | $Co_{0.14}/N_{0.11}C$ (2 cycle) | 160 | 8 | 99 |
| 3 | $Co_{0.14}/N_{0.11}C$ (3 cycle) | 160 | 8 | 50 |
| 4 | $Co_{0.14}/N_{0.11}C$ (4 cycle) | 160 | 8 | 46 |
| 5 | $Co_{0.14}/N_{0.11}C$ (0.1 NaOH) | 160 | 8 | 48 |

**Dehydrogenation condition:** 0.1 mmol of 1, 2, 3, 4-tetrahydroquinoline, 100 mg of catalyst, 160 °C and 30 bar of Ar gas.

# References

[S1] J. P. Perdew, K. Burke, M. Ernzerhof, *Phys. Rev. Lett.* 1996, **77**, 3865-3868.

[S2] B. Delley, *J. Chem. Phys.* 1990, **92**, 508-517.

[S3] B. Delley, *J. Chem. Phys.* 2000, **113**, 7756-7764.

[S4] Q. Li, Z. Wang, Z. Lin, Y. He, K. Zhang, R. Whiddon, K. Cen, *Energy Fuels*, 2016, **30**, 8125-8133.

[S5] Y. Han, Z. Wang, R. Xu, W. Zhang, W. Chen, L. Zheng, J. Zhang, J. Luo, K. Wu, Y. Zhu, C. Chen, Q. Peng, Q. Liu, P. Hu, D. Wang, Y. Li, *Angew. Chem. Int. Ed.*, 2018, **57**, 11262-11266.

[S6] Z. Wei, Y. Chen, J. Wang, D. Su, M. Tang, S. Mao, Y. Wang, *ACS Catal.* 2016, **6**, 5816-5822.

[S7] F. Chen, A. E. Surkus, L. He, M. M. Pohl, J. Radnik, C. Topf, K. Junge, M. Beller, *J. Am. Chem. Soc.* 2015, **137**, 11718-11724.

[S8] R. Xu, S. Chakraborty, H. Yuan, W. D. Jones, *ACS Catal.* 2015, **5**, 6350-6354.

[S9] R. Adam, J. R. Cabrero-Antonino, A. Spannenberg, K. Junge, R. Jackstell, M. Beller, *Angew. Chem. Int. Ed.* 2017, **56**, 3216-3220.

[S10] P. Ryabchuk, A. Agapova, C. Kreyenschulte, H. Lund, H. Junge, K. Junge, M. Beller, *Chem. Commun.,* 2019*, **55**,* 4969-4972.

[S11] K. Kaneda, Y. Mikami, T. Mitsudome, T. Mizugaki, K. Jitsukawa, *Heterocycles*, 2010, **82**, 1371-1377.